INTERNATIONAL JOURNAL FOR NUMERICAL METHODS IN FLUIDS
Int. J. Numer. Meth. Fluids 2008; **56**:1217–1223
Published online in Wiley InterScience (www.interscience.wiley.com). DOI: 10.1002/fld.1732

Combining CVFEM and meshless front tracking in Hele–Shaw mold filling simulation

K. C. Estacio[1,*,†], L. G. Nonato[1], N. Mangiavacchi[2] and G. F. Carey[3]

[1]*Instituto de Ciências Matemáticas e de Computação, ICMC/USP, 13560-970, São Carlos-SP, Brazil*
[2]*Faculdade de Engenharia, FEN/UERJ, 20550-900, Rio de Janeiro-RJ, Brazil*
[3]*Institute for Computational Engineering and Sciences, University of Texas, Austin, TX 78712, U.S.A.*

SUMMARY

In this work, a generalized Hele–Shaw approach is developed for non-isothermal, non-Newtonian and inelastic flows arising in injection molding. The advancing free surface of the injected fluid is predicted by a novel meshless front-tracking method coupled to control volume finite element solution for the pressure. A modified Cross constitutive model with Arrhenius temperature dependence is employed to describe the viscosity of the melt and the temperature field is solved by a semi-Lagrangian scheme with a finite volume method. The utility of the combined algorithm is demonstrated for a test problem that has complex 'obstacles' in the mold interior. Copyright © 2008 John Wiley & Sons, Ltd.

Received 30 April 2007; Revised 29 November 2007; Accepted 5 December 2007

KEY WORDS: meshless front tracking; Hele–Shaw; CVFEM; non-Newtonian; semi-Lagrangian

1. INTRODUCTION

Contemporary polymer processing simulation needs for injection molding applications require non-Newtonian, non-isothermal capabilities. These should be integrated with more flexible mesh and discretization approaches to address complex geometry and advancing free boundaries. Slow viscous flow in a mold with relatively narrow gaps may be modeled reliably by a Hele–Shaw approximation [1, 2]. Moreover, viscous heating plays an important role in the overall energy balance for thin mold parts, whereas melt elasticity has little influence on injection pressures and

*Correspondence to: K. C. Estacio, Instituto de Ciências Matemáticas e de Computação, ICMC/USP, Av. Trabalhador São-carlense, 400, 13560-970, São Carlos-SP, Brazil.
†E-mail: kemelli@icmc.usp.br

Contract/grant sponsor: FAPESP; contract/grant number: 05/51040-6
Contract/grant sponsor: Capes; contract/grant number: BEX4705/06-8
Contract/grant sponsor: CNPq; contract/grant numbers: 307230/06-6, 486153/06-1
Contract/grant sponsor: FURNAS Centrais Elétricas S/A

fill rates so that generalized viscosity models such as the Cross model [3] considered here are applicable. These features of the mold-filling problem provide several simplifications of the underlying 3D-coupled multiphysics process that leads to a less complex model that can be addressed by an efficient iteratively decoupled algorithm as developed here. The numerical method developed in this work utilizes the singular handle edge data structure [4] for a background unstructured Delaunay triangulation [5] to construct a control volume finite element method (CVFEM) [6, 7]. The moving free surface is computed using a novel point-based local meshfree modification of the front-tracking method. This scheme has the advantage of both allowing more than one control volume to be filled at each time step when compared with the volume of fluid method proposed in [7] and avoiding the explicit treatment of topological changes in the surface, usually an issue found in purely front-tracking methods [8].

2. COUPLED NON-NEWTONIAN HELE–SHAW SYSTEM

As indicated in the Introduction, for the class of moving boundary problems considered here, model simplification leads to a quasi-steady 2D Hele–Shaw system for pressure coupled to a 3D heat transfer model. The Hele–Shaw equation for pressure in an incompressible generalized Newtonian fluid with constant thermal conductivity has the form:

$$\nabla \cdot S_2 \nabla p = 0 \tag{1}$$

where p is the pressure and, in symmetric flow fields, $S_2 = \int_0^h \frac{z'^2}{\eta}\,\mathrm{d}z'$, for generalized viscosity η and mold thickness h. The pressure equation above is coupled to the energy equation:

$$\rho c_p \left(\frac{\partial T}{\partial t} + \mathbf{v} \cdot \nabla T \right) = \eta \dot{\gamma}^2 + k \frac{\partial^2 T}{\partial z^2} \tag{2}$$

where T denotes temperature, c_p is the specific heat at constant pressure, $\mathbf{v}$ is the velocity in the xy-plane, $\dot{\gamma}$ is the shear rate and k is the thermal conductivity. Convection in the z-direction, being small, is neglected. The remaining components v_x and v_y of the velocity are

$$v_x = -\frac{\partial p}{\partial x}\left(\int_0^z \frac{z'}{\eta}\,\mathrm{d}z' - \int_0^h \frac{z'}{\eta}\,\mathrm{d}z' \right) \quad \text{and} \quad v_y = -\frac{\partial p}{\partial y}\left(\int_0^z \frac{z'}{\eta}\,\mathrm{d}z' - \int_0^h \frac{z'}{\eta}\,\mathrm{d}z' \right) \tag{3}$$

The pressure equation (1) and energy equation (2) are coupled through the convective velocity and by the dependence of the viscosity on both temperature and shear rate. In the present study, a modified Cross model with Arrhenius temperature dependence [3] is implemented:

$$\eta(T, \dot{\gamma}) = \frac{\eta_0(T)}{1 + \left(\eta_0 \dfrac{\dot{\gamma}}{\tau^*} \right)^{1-n}} \quad \text{with } \eta_0(T) = B \exp\left(\frac{T_b}{T} \right) \tag{4}$$

where n is the power law index, η_0 is the zero-shear viscosity, τ^* is the parameter that defines the transition region between zero shear rate and the power law region of the viscosity curve and B and T_b are constants that depend on the fluid. Boundary and initial conditions for pressure, flow rate and temperature complete the mathematical model as described for the test case in the results section.

DOI: 10.1002/fld

3. DECOUPLED ALGORITHM AND FRONT STRATEGY

The numerical algorithm involves time integration of the energy equation coupled with solution of the Hele–Shaw pressure equation. Since the timescale for the energy equation is larger than for the hydrodynamics, an iterative decoupled scheme is appropriate with the temperature field for the pressure equation taken from the previous step of the energy solver. Iteratively decoupled approximation of the pressure and temperature field equations is followed by advancement of the free surface using a front-tracking approach with a local 'meshless' data structure at the front.

3.1. Control volume finite element discretization of the pressure equation

A background 2D Delaunay triangulation of the midplane mold domain is first generated. This is then used to construct a mesh of non-overlapping medial finite volumes. The discretization of Equation (1) using the CVFEM follows on application of the Gauss divergence theorem to the corresponding integral conservation statement for each volume. We obtain

$$\int_V \nabla\cdot(S_2\nabla p)\,\mathrm{d}V=\int_S (S_2\nabla p)\cdot\mathbf{n}\,\mathrm{d}S=0$$

where S is the closed boundary of finite volume V and $\mathbf{n}$ denotes the unit outward vector normal to S. In the present scheme, a linear pressure approximation is assumed on each triangle of the underlying Delaunay mesh. The associated boundary integral contributions from medial segments are accumulated and assembled to a sparse algebraic system which is solved using the conjugate gradient method [7].

3.2. Solution of the energy equation

First, recall that convection in the vertical direction is small and therefore neglected, but conduction in the horizontal direction is included. A semi-Lagrangian formulation in the plane may then be introduced to accommodate convection [9]. Introducing the material derivative, the energy equation (2) is rewritten as

$$\frac{\mathrm{D}T}{\mathrm{D}t}=f \quad \text{where } f=\frac{1}{\rho c_p}\left(\eta\dot{\gamma}^2+k\frac{\partial^2 T}{\partial z^2}\right) \tag{5}$$

In the discrete model, we consider the tensor product of the mold midplane triangulation with a 1D mesh in the vertical direction. Conduction in the z-direction through the advancing thin fluid layer is discretized by 1D finite differencing, using a pre-defined number of layers. For the convective transport in the discretized semi-Lagrangian scheme, consider a particle that occupies the position of a planar mesh vertex $\mathbf{x}$ at time $t+\delta t$ (and that had previously occupied position $\mathbf{x}-\delta\mathbf{x}$ at time t). The material derivative may then be discretized accordingly through this time interval δt. Then expanding $T(\mathbf{x}-\delta\mathbf{x},t)$ in a truncated Taylor expansion and substituting in the previous expression, we obtain

$$T(\mathbf{x},t+\delta t)=T(\mathbf{x},t)-\delta t\,\mathbf{v}\cdot\nabla T+\delta t f \tag{6}$$

where ∇T is computed for the element that contains the particle of fluid at time t, and $\mathbf{v}$ is the velocity at the vertex. The Cross fluid viscosity relation and Arrhenius model introduce nonlinearities in the resulting discretized algebraic system at each implicit timestep and are solved by

DOI: 10.1002/fld

Newton's method. A more detailed description of the solution scheme for the energy equation (2) is given by Estacio and Mangiavacchi [7].

3.3. Modified front-tracking 'meshless' free surface representation

The discretized free surface can be modeled by a subset of points moving with the local velocity of the front across a fixed background mesh. Topological changes in the surface, such as coalescence and splitting may be conveniently accommodated through a flexible data structure that identifies local nearby one-sided point clusters at the front. This may be viewed in some sense as a front-tracking strategy combined with a local meshless construct along the fluid side of the advancing front. Since point distribution can rapidly change during the simulation, the method must be able to handle both insertion and removal of points, so as to preserve the quality of the front. This aspect of the algorithm involves a local spatial search adjacent to the moving front with marking of triangular background elements that contain the points of the front: for each point p of the front, a radius defining the neighborhood of the point is computed from the average of the edge lengths of the triangle containing the point, to find its neighbor points in the front and its nearest neighbor, n_p. Then, the angles formed among p and its neighbors are calculated and used to compose 1D cluster(s) [10] corresponding to neighbor points on the front on either side of p as follows: the angles formed by connecting p to its nearest neighbor n_p and then connecting p with all others neighbors n_i, $i=1\ldots N$, where N is the number of neighbors, are computed. If these angles are smaller than a threshold, ε, then neighbors of p are grouped into the same cluster; otherwise, they are grouped in two clusters, as illustrated in Figure 1.

If a point p gives rise to only one cluster, it implies that p is a border of the free surface, while two clusters mean that it is in the interior of the front and this information defines the insertion

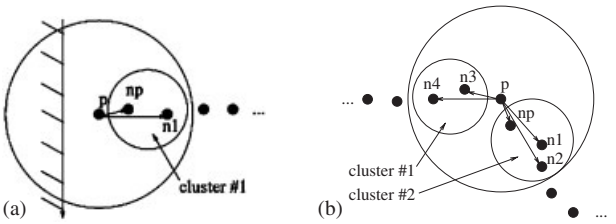

Figure 1. The angle $n_p p n_1$ is small in (a), implying one cluster, whereas in (b) the angles $n_p p n_1$ and $n_p p n_2$, are small but the angles $n_p p n_3$ and $n_p p n_4$ are large implying two clusters.

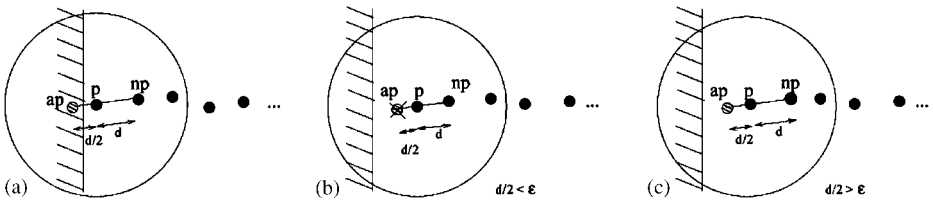

Figure 2. Insertion procedures for border points: the method seeks to insert a new point ap in the direction opposite the vector from p to np. In (a) and (b), insertion is not accomplished because the new point is outside the domain and the distance between p and ap is smaller than the tolerance ε, respectively. Insertion is successfully accomplished in (c).

DOI: 10.1002/fld

strategy. In the case of border points, the algorithm tries to insert a new point ap in the direction opposite to a vector from p to its nearest neighbor np. The distance from p to this new point is prescribed as equal to half the distance between p and np as illustrated in Figure 2. If the point ap lies outside the domain, it is not included in the updated front; also, if the distance between the new point ap and p is smaller than a predefined threshold, it is likewise deleted. Finally, if the point is neither outside the domain nor too close to p, it will be added to the front and marked as a new border of the free surface.

In case of insertion in the interior of the front, the process is accomplished as follows: if the distance from p to its nearest neighbor in each cluster is larger than half the circle radius, then a new point is inserted between p and its neighbor. Point removal is carried out if the distance from p to its nearest neighbor is smaller than a pre-defined tolerance.

4. NUMERICAL RESULTS

Numerical results for a representative test case are presented here to demonstrate the utility of the scheme, study the coupled transport processes and examine the behavior of the front treatment. The test case geometry corresponds to a rectangular mold with several geometrical interior 'obstacles' as shown in Figure 3. The corresponding unstructured background Delaunay mesh has 4677 elements and 2513 finite volume polygon dual cells. Horizontal flow velocity and temperature are specified at the mold inlet as $v_0 = 10^{-1}$ m/s and $T = 513$ K, respectively. The reference wall temperature is $T_w = 313$ K and the reference pressure is $p_0 = 10^5$ N/m^2. For polystyrene, material constants in the modified Cross model are $n = 0.2838$, $\tau^* = 1.791 \times 10^4$ Pa, $T_b = 11\,680$ K and $B = 2.591 \times 10^{-7}$ Pa s. The density, the specific heat and the thermal conductivity are, respectively, $\rho = 940$ Kg/m^3, $c_p = 2100$ J/Kg K and $k = 0.18$ W/m K [11].

The time to complete injection of the specified mold volume at the given inlet flow rate is 1.43 s. Figures 4–6 show the pressure field, temperature field and the front location, respectively, at intermediate times $t = 0.16$, 0.31, 0.37, 0.50, 0.67, 0.97, 1.16 and 1.27 s.

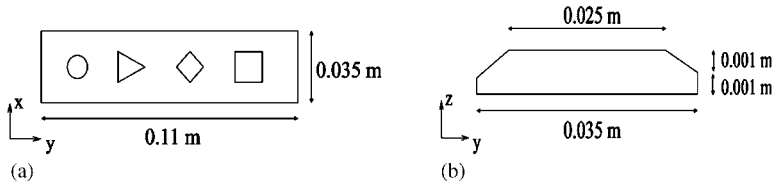

Figure 3. Dimensions of mold with interior 'obstacles': (a) top view and (b) lateral view.

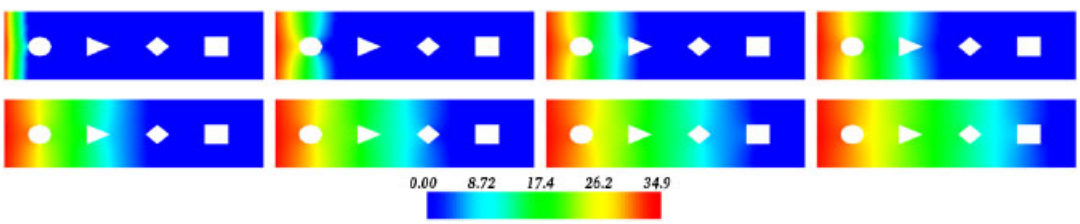

Figure 4. Evolution of the pressure field. Values are scaled by p_0.

DOI: 10.1002/fld

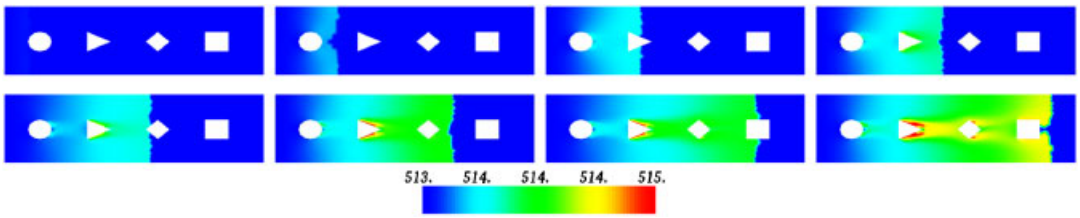

Figure 5. Evolution of temperature field.

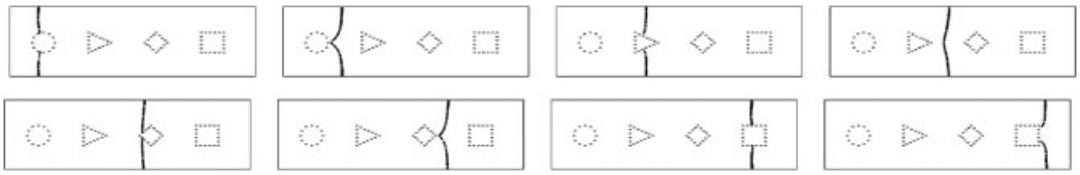

Figure 6. Advancement of fluid front.

As expected, the pressure drop is higher around the inlet and the fluid is at a higher temperature closer to the 'obstacles' due to the shear viscous effects. An accurate solution of the 3D temperature equation is important because it will affect viscosity of the polymer and, therefore, velocity, front position and pressure distribution [12].

In this simulation, it is also possible to observe the capability of the present model to deal with splitting and remerging of the free surface during the filling process, with addition or removal of fluid front particles where needed. Adequate characterization of this effect is essential to guarantee the final quality of the mold part, since the remerging regions correspond to the most fragile areas of the molded part.

The profiles for pressure, temperature field and fluid front position shown above are quantitatively similar to those obtained when the VOF scheme in [7] is used to track the free surface. However, the VOF implementation requires 2476 iterations and 8 min 48 s on an Intel Xeon Quad-Core 3.2 GHz processor with 4 GB RAM, whereas the present method with CFL = 0.5 requires 127 iterations and takes 3 min 7 s.

5. CONCLUSION

A novel Hele–Shaw scheme for mold filling is developed that involves a 2D model for the pressure equation of a generalized Newtonian fluid coupled with a 3D thermal model. This model permits an iteratively decoupled solution strategy within each timestep of a meshless moving front algorithm. The pressure discretization employs an unstructured control volume scheme, and in the energy equation, convective heat transfer in the plane is accommodated using a semi-Lagrangian discretization. The resulting solution algorithm is applied to a representative mold-filling problem and shown to give accurate reliable results as compared with a prior volume of fluid scheme in the literature but requiring less computer time.

DOI: 10.1002/fld

REFERENCES

1. Hieber CA, Shen SF. A finite-element/finite-difference simulation of the injection-molding filling process. *Journal of Non-Newtonian Fluid Mechanics* 1980; **7**:1–32.
2. Tucker CL. *Computer Modeling for Polymer Processing—Fundamentals*. Hanser Publishers: Munich, 1989.
3. Cross MM. Kinetic interpretation of non Newtonian flow. *Journal of Colloid and Interface Science* 1970; **33**:30–35.
4. Nonato LG, Castelo A, Lizier MAS, Oliveira MCF. Topological approach for detecting objects from images. *Vision Geometry XII—Proceedings Electronic Imaging* 2004; **5300**:62–73.
5. Easymesh: a free two-dimensional quality mesh generator based on Delaunay triangulation. http://www-dinma.univ.trieste.it/nirftc/research/easymesh/ [12 September 2007].
6. Baliga BR, Patankar SV. A new finite element formulation for convection–diffusion problems. *Numerical Heat Transfer* 1981; **3**:393–409.
7. Estacio KC, Mangiavacchi N. Simplified model for mold filling simulations using CVFEM and unstructured meshes. *Communications in Numerical Methods in Engineering* 2007; **23**(5):345–361.
8. Glimm J, Grove J, Lindquist WB, McBryan O, Tryggvason G. The bifurcation of tracked scalar waves. *SIAM Journal on Scientific and Statistical Computing* 1988; **9**(1):61–79.
9. Phillips TN, Williams AJ. A semi-Lagrangian finite volume method for Newtonian contraction flows. *SIAM Journal on Scientific Computing* 2001; **6**(22):2152–2177.
10. Jain AK, Murty MN, Flynn PJ. Data clustering: a review. *ACM Computing Surveys* 1999; **31**:264–323.
11. Chen SC, Chen YC, Cheng NT. Simulation of injection–compression mold-filling process. *International Communication in Heat and Mass Transfer* 1998; **25**(7):907–917.
12. Ahn H, Carey GF. An enhanced polygonal finite volume method for unstructured hybrid meshes. *International Journal for Numerical Methods in Fluids* 2007; **54**(1):29–46.

DOI: 10.1002/fld